

# RSC Advances



This is an *Accepted Manuscript*, which has been through the Royal Society of Chemistry peer review process and has been accepted for publication.

*Accepted Manuscripts* are published online shortly after acceptance, before technical editing, formatting and proof reading. Using this free service, authors can make their results available to the community, in citable form, before we publish the edited article. This *Accepted Manuscript* will be replaced by the edited, formatted and paginated article as soon as this is available.

You can find more information about *Accepted Manuscripts* in the [Information for Authors](#).

Please note that technical editing may introduce minor changes to the text and/or graphics, which may alter content. The journal's standard [Terms & Conditions](#) and the [Ethical guidelines](#) still apply. In no event shall the Royal Society of Chemistry be held responsible for any errors or omissions in this *Accepted Manuscript* or any consequences arising from the use of any information it contains.

# Synthesis of B-doped hollow carbon spheres as efficient non-metal catalyst for oxygen reduction reaction

Cite this: DOI: 10.1039/x0xx00000x

Hui-Jia Lu, Ying Li\*, Lin-Qun Zhang, He-Nan Li, Zhi-Xin Zhou, An-Ran Liu, Yuan-Jian Zhang, Song-Qin Liu\*

The oxygen reduction reaction (ORR) is one of the crucial reactions in fuel cells and metal-air batteries. Heteroatom doped carbon spheres can be served as alternative low-cost non-metal electrocatalysts for ORR. Here, we developed an effective route to the synthesis of uniform and electrochemically active B-doped hollow carbon nanospheres (BHCSs). BHCSs were synthesized via carbonization of boric phenolic resin supported by SiO<sub>2</sub>, followed by etching the SiO<sub>2</sub> template. The content of B, B dopant species and specific surface area were adjusted by changing the content of B precursor and calcination temperature. Moreover, their influences on the performances of electrocatalytic activity were explored. It was found that that, among these B-doping types (BC<sub>2</sub>O, BCO<sub>2</sub>, B<sub>4</sub>C and BC<sub>3</sub>), B-C bonds (B<sub>4</sub>C and BC<sub>3</sub>) played a crucial role on improving the electrocatalytic activity. Compared with the hollow carbon nanospheres (HCSs), a 70 mV positive shift of the onset potential and 1.7 times kinetic current density can be clearly observed on BHCSs. In addition, the BHCSs revealed better stability and methanol tolerance than commercial Pt/C (HiSPEC™ 3000, 20%). Thus, the as-prepared BHCSs, as the inexpensive and efficient non-metal ORR catalysts, may have a promising application in direct methanol fuel cells.

Received 00th January 2012,  
Accepted 00th January 2012

DOI: 10.1039/x0xx00000x

[www.rsc.org/](http://www.rsc.org/)

## Introduction

The oxygen reduction reaction (ORR), a key process in metal-air batteries and fuel cells, is kinetically sluggish, thus similarly, appeals for a suitable catalyst.<sup>1-5</sup> To date, Pt-based electrocatalysts become the popular materials for ORR with high current density and four-electron pathway.<sup>6-8</sup> However, they still suffer from the poor stability, CO and methanol poisoning. Furthermore, the high cost and the limited natural resource of Pt have blocked its large-scale application.<sup>9,10</sup> In this respect, non-metal carbon-based catalysts have attracted a great attention due to their outstanding stability, low cost, good methanol and CO tolerances and high electrocatalytic activity.<sup>11,12</sup>

The electrons in the sp<sup>2</sup> carbon materials are too inert to be utilized directly in ORR.<sup>13</sup> Doped with heteroatom in carbon framework, the carbon electrons have been activated; thus, O<sub>2</sub> molecules can be reduced on the positively charged atoms.<sup>14</sup> When a heteroatom is bonded with the carbon framework, it can introduce a defect in the adjacent sites due to the difference in atomic size and bond length.<sup>15,16</sup> Moreover, the electronegativity of different atoms can make uneven charge

distribution.<sup>17,18</sup> Therefore, the heteroatom-doped carbon have been pioneered for ORR electrocatalysts.<sup>19-29</sup> Specially, because C has larger electronegativity (2.55) than B (2.04), an amount of positive charge was induced to the B atoms. These B atoms are favorable to capturing the oxygen molecules.<sup>30</sup> Besides, once the B doped into the carbon matrix, the electrons of C-C  $\pi^*$  orbital would transfer to vacant 2p<sub>z</sub> orbital of B. Hu et al. found that this partially filled 2p<sub>z</sub> orbital makes up the main protruding lobe in the two highest occupied molecular orbitals (HOMO) of BHCSs.<sup>31</sup> Upon adsorption, the lowest unoccupied molecular orbital (LUMO) of oxygen would overlap with the HOMO of BHCSs. As a result, an amount of charge transfers to oxygen, causing the stretch of the O-O bond length. The weakness of O-O bond makes the reduction of oxygen more efficiently. These B-doped carbon materials can increase the electrocatalytic performance for ORR. B doped carbon materials, such as graphene,<sup>28</sup> carbon nanotubes,<sup>31</sup> ordered mesoporous carbons,<sup>32</sup> and carbon rods,<sup>33</sup> can increase the electrocatalytic performance for ORR.

Hollow carbon spheres (HCSs) have been paid considerable attention to because of their superior properties such as low density, high specific surface area, good chemical stability and electrical conductivity. These features guarantee them

promising in drug delivery, catalysis, energy conversion and storage.<sup>34-36</sup> The high specific surface area of HCSs facilitates the exposure of active sites for catalysis. Up to now, most synthetic routes of doped HCSs through two main approaches: the first through a one-step pyrolysis of heteroatom contained carbon precursor, and the second through post-treatment of HCSs with reactive heteroatom precursor.<sup>37</sup> However, to our best knowledge, no report has researched the B-doped hollow carbon spheres catalyst for ORR.

Herein, we report a catalyst-free and facile approach to synthesize B-doped hollow carbon spheres (BHCSs). BHCSs were prepared using SiO<sub>2</sub> spheres as the hard template, 4-hydroxyphenylboronic acid as B source, resorcinol and methanol as carbon source. In this process, rather than simply physical mixture, 4-hydroxyphenylboronic acid was added into phenol to react to produce boric phenyl ester, which further reacted with formaldehyde to form boric phenolic resin.<sup>38</sup> The Scheme 1 shows the schematic illustration of the formation process of the BHCSs, including hydrothermal reaction, carbonization, and HF etching. The resulting BHCSs own superior electrochemical performance for ORR. As metal-free catalysts, BHCSs show much better long-term durability, methanol tolerances than the commercial Pt/C (HiSPEC™ 3000, 20%) in alkaline medium.



**Scheme 1** Schematic illustration of the formation process of the B-doped hollow carbon spheres (BHCSs)

## Experimental

### Chemicals

Tetraethyl orthosilicate (TEOS) (99%) was purchased from Aldrich (China). Resorcinol and formaldehyde (37 wt%) were bought from Sinopharm Chemical Reagent Co. Ltd. (China). 4-hydroxyphenylboronic acid was purchased from Ningbo Yingfa Pengna. Ltd. (China). Commercial 20 wt% Pt/C (HiSPEC™ 3000) was from Johnson Matthey. Other chemicals such as ammonia solution (28 %), potassium hydroxide and ethanol were from Sinopharm Chemical Reagent Co. Ltd (China). All the reagents were of analytical grade and used as received. All solutions used in the experiments were freshly prepared with ultrapure water having a resistivity of 18.2 MΩ cm<sup>-1</sup> (Nanjing Baocheng Biotechnology CO. Ltd., China).

### Preparation of HCSs and BHCSs

Here, we synthesised the HCSs by using SiO<sub>2</sub> as templates, resorcinol–formaldehyde as carbon source according to literature.<sup>39</sup> In this synthesis process, silica colloidal spheres were first formed via the classical Stöber method,<sup>40</sup> and then acted as cores for the deposition of resorcinol–formaldehyde shells. HCSs were prepared according to the method reported by Dongyuan Zhao.<sup>35</sup> Generally, 4.25 mL of TEOS mixed with 75 mL of ethanol was added to a solution containing 50 mL of ethanol, 15 mL of ultrapure water and 10 mL of ammonia aqueous solution under stirring. After 1 h, 1 g of resorcinol and 1.4 mL of formaldehyde solution were added, respectively. The solution was stirred for 24 h at room temperature, then transferred to a 250 mL Teflon-lined stainless steel autoclave, and hydrothermally treated for 24 h at 100 °C. After cooling down, the solid product was obtained by centrifugation and desiccation at 60 °C overnight. Then as-prepared carbon spheres were thermally in a tube furnace with a heating rate of 5 °C min<sup>-1</sup> under nitrogen atmosphere until a final temperature was reached and then the samples were kept for 4 h. The samples were cooled down naturally to room temperature. After the composites immersed in 10 wt% HF solutions for 36 h, the SiO<sub>2</sub> colloidal cores were removed and HCSs were obtained. The preparation of B-doped HCSs was performed by using 4-hydroxyphenylboronic acid partly instead of resorcinol for preparation of HCSs. The total amount of 4-hydroxyphenylboronic acid and resorcinol was controlled to 1 g with different mass ratio. The obtained BHCSs were boiled in deionized water at 100 °C for 6 h to dissolve the B that had not been doped into the carbon framework. In this paper, we name the samples with BHCSs-*m-n*, in which *m* represents the mass percent of 4-hydroxyphenylboronic acid, while *n* represents the different calcination temperature.

### Apparatus

The surface morphologies of the samples were analyzed by field emission scanning electron microscopy (FE-SEM) using an ULTRA plus microscope (Zeiss, Germany) and a JEM-2100 field emission transmission electron microscopy (FE-TEM, JEOL, Japan) with an acceleration voltage of 200 kV. Particle size distribution was obtained by dynamic light scattering analysis (DLS, Brookhaven BI-200SM, USA). Raman spectra were collected by DXR-Microscope (Thermo Fisher, USA) with the excitation wavelength of 532 nm. Nitrogen sorption isotherms and Brunauer–Emmett–Teller (BET) surface areas were investigated by NovaWin (Quantachrom, USA). Thermogravimetric (TG) was performed on the SDT-Q600 thermal analyzer (TA Instruments, USA) in an N<sub>2</sub> atmosphere at a heating rate of 20 °C min<sup>-1</sup> with temperature ranging from 50 to 900 °C. X-ray photoelectron spectroscopy (XPS) was performed by a PHI5000 VersaProbe (Ulvac-Phi, Japan) system with a monochromic Mg-Kα radiation. All the electrochemical measurements were performed on a CHI700 electrochemical workstation (CH Instruments, China) and Rotating Ring Disk Electrode (RRDE-3A, Japan) in a typical three-electrode cell equipped with gas flow systems. A glassy carbon electrode

(GCE) with a diameter of 3 mm was used as the working electrode. While a platinum filament and Ag/AgCl (saturated KCl) were used as the counter electrode and reference electrodes, respectively. All electrochemical experiments were carried out at room temperature. GCE was polished successively with 1.0 and 0.3  $\mu\text{m}$  alumina powders before modification, rinsed with ethanol/water and twice-distilled water thoroughly, followed by drying under a stream of nitrogen. 4 mg of BHCSs was ultrasonically dispersed in 1 mL ethanol to form homogeneous BHCSs suspensions. Then 10  $\mu\text{L}$  this suspension was cast on the GCE surface, dried at 60  $^{\circ}\text{C}$  oven for 15 min. After that, 5  $\mu\text{L}$  of Nafion (0.05 wt% in ethanol) was cast on the GCE surface and allowed to dry at 60  $^{\circ}\text{C}$  oven for another 15 min to obtain BHCSs modified GCE. For all the cyclic voltammograms and rotating disk electrode (RDE), the loading of catalysts was 0.28  $\text{mg cm}^{-2}$  for Pt/C and 0.56  $\text{mg cm}^{-2}$  for HCSs and BHCSs. The electrolyte was 0.1 M KOH in water, which was bubbled with  $\text{O}_2$  or  $\text{N}_2$  for 30 min and maintained with the same atmosphere during the measurements. Cyclic voltammetry (CV), linear sweep voltammetry (LSV) and chronoamperometry were carried out to measure the catalytic performances of the BHCSs for ORR. All current densities were normalized to the geometric surface area of the GCE. The capacitive current densities were subtracted from the apparent current densities by deducting the background current density obtained from the deoxygenated electrolyte.

## Results and discussion

### Characterization of the BHCSs

Here, the sample BHCSs-0.3-900 is taken as an example. The colloidal  $\text{SiO}_2$  nanospheres prepared by a classical Stöber method are smooth and monodispersed with a uniform diameter of  $\sim 170$  nm (Fig. S1a, ESI $\dagger$ ). A further modified coating process and hydrothermal reaction lead to form B doped carbon spheres with a diameter of  $\sim 230$  nm (Fig. S1b, ESI $\dagger$ ). The *in situ* polymerization was induced by the  $\text{NH}_4^+$  ions, decorated on the surface of the  $\text{SiO}_2$  spheres under basic conditions, which could not only prevent the colloidal suspension from aggregating but also accelerate the polymerization of boric phenolic resin.<sup>41</sup> The B doped carbon spheres retain the original core-shell structure after a heat treatment but the diameter is reduced to  $\sim 200$  nm (Fig. 1a and b), indicating an apparent structure shrinkage during the carbonization. Removing of the silica cores by an etching treatment, the SEM image showed that the resulting BHCSs-0.3-900 retained well the spherical morphology with no obvious collapse observed (Fig. 1c), implying that this hollow structure may possess great mechanical strength. TEM image of the BHCSs-0.3-900 clearly exhibits hollow nanostructures with a shell thickness of  $\sim 15$  nm and a void of  $\sim 170$  nm in diameter (Fig. 1d), which is agreement with the diameter of the  $\text{SiO}_2$  cores. The DLS data further confirms that the BHCSs-0.3-900 nanospheres have a narrow size distribution (Fig. S2a, ESI $\dagger$ ).

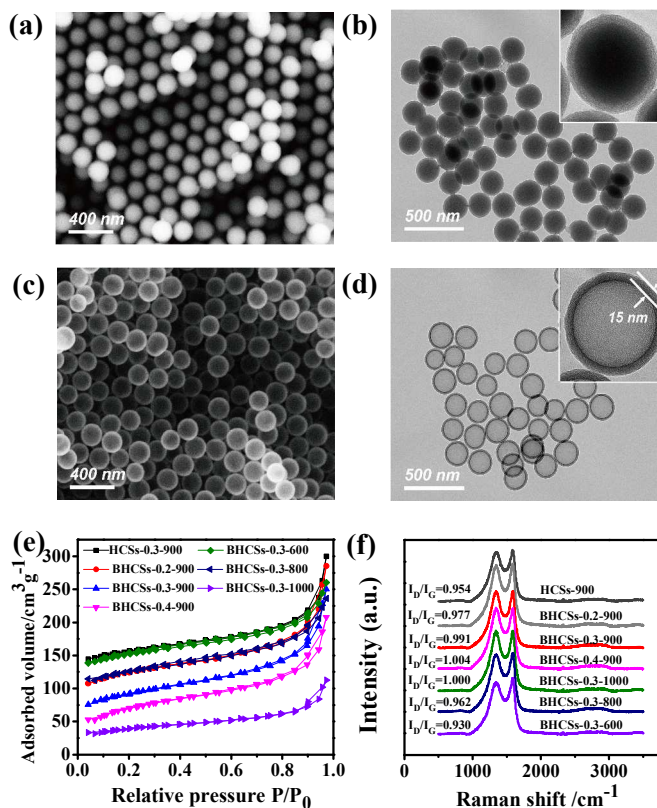


**Fig. 1** SEM (a and c) and TEM (b and d) images of the BHCSs before (a and b) and after (c and d) colloidal  $\text{SiO}_2$  cores removal. (e) Nitrogen adsorption–desorption isotherms of HCSs-900 and various BHCSs samples. (f) Raman spectra of HCSs-900 and various BHCSs samples.

Nitrogen sorption measurement shows that that HCSs-900 possessed microporous structure and the specific surface reaches  $478.31 \text{ m}^2 \text{ g}^{-1}$  (Fig. 1e). The specific surface area of the BHCSs-0.3-900 is smaller than HCSs-900, indicating that B is successfully doped into HCSs. The introduction of B into the framework of HCSs leads to decrease the specific surface area.<sup>32</sup> On the other hand, the samples calcined at relative high temperature show relatively low specific surface area. High annealing temperature may lead to the collapse of the micropores. The detail informations of the samples are summarized in Table 1. According to thermogravimetric analysis in  $\text{N}_2$  (Fig. S2b), a three-step weight loss process could be observed for both HCSs and BHCSs-0.3-900. The majority of chemicals decomposition takes place from 400–900  $^{\circ}\text{C}$ , this weight loss may be attributed to a suite of complex chemical reactions, involving bond formation and crosslinking,<sup>24</sup> which result in the destruction of main chain and the release of small gases ( $\text{CO}$ ,  $\text{CO}_2$ ,  $\text{CH}_4$  and  $\text{H}_2$ ).<sup>43</sup> However, there is no obvious mass loss at higher temperatures 800–900  $^{\circ}\text{C}$  for BHCSs, indicating that the BHCSs possess higher heat resistance and carbon yield. Raman spectroscopy is the most effective technique to characterize the structure, determine the defects

and disordered structures. The Raman spectra of the HCSs-900 and BHCSs-0.3-900 exhibit the presence of two strong bands at 1350 and 1590  $\text{cm}^{-1}$ , respectively, corresponding to the D and G bands (Fig. 1e). Although there are no apparent changes in the positions of the D and G bands between BHCSs and HCSs, BHCSs (except BHCSs-0.3-600) show higher intensity ratios of  $I_D/I_G$ , due to the introduction of defects in the carbon framework by the heterogeneous B-dopants. Notably, the  $I_D/I_G$  ratio of BHCSs gradually increases on raising the annealing temperature, suggesting that higher annealing temperature could induce more defects.<sup>42</sup>

**Table 1.** Properties of HCSs and BHCSs

Catalyst	Mass of B source	BET Surface area ( $\text{m}^2\text{g}^{-1}$ )	XPS (at. %)		
			C	B	O
HCS-900	0.0	478.31	96.55	-	3.45
HCS-0.2-900	0.2	395.56	91.55	0.61	7.84
HCS-0.3-900	0.3	307.27	90.94	0.91	8.15
HCS-0.4-900	0.4	242.17	89.94	1.08	8.98
HCS-0.3-1000	0.3	131.08	92.31	0.41	7.28
HCS-0.3-800	0.3	395.22	90.25	1.12	8.63
HCS-0.3-600	0.3	468.77	89.17	1.36	9.47

The elemental compositions and chemical bonding information of HCSs and BHCSs were investigated via XPS measurements. The XPS survey for BHCSs shows a clear B band emerged in BHCSs, confirmed that B is successfully doped into HCSs and the silica have been etched absolutely (Fig. 2a). The atomic contents of C, B, and O in the samples are summarized in Table 1. It is found that the content of B and O increase as the initial mass of 4-hydroxyphenylboronic acid increasing, which is agreement with the B-doped materials.<sup>32</sup> Based on the Gauss Amp, the B 1s peak in BHCSs can be fitted into four components (Fig. 2b). The peaks center at 187.5 eV and 189.5 eV may be assigned to  $\text{B}_4\text{C}$  and  $\text{BC}_3$  structures, respectively. The peaks at 191.2 eV and 192.3 eV correspond to  $\text{BC}_2\text{O}$  and  $\text{BCO}_2$ , respectively.<sup>31,32,44</sup> Previous studies demonstrated that the variation in the amount of B-C is allegedly responsible for the ORR activity.<sup>31,33</sup> The B doping sites of  $\text{BC}_2\text{O}$  and  $\text{BCO}_2$  are on the edge of the carbon framework and these two doped types, particularly  $\text{BCO}_2$ , may make negative influences on the electronic conductivity of the samples.<sup>45</sup> The  $\text{BC}_3$  species containing in BHCSs improving the ORR activity is demonstrated by follow electrochemical measurements. The potential schematic structure of the BHCSs is outlined in Figure 2c. The content of each B species is listed in Table 2. It can be seen that, with the increase of the calcination temperature, the bands belong to B-C ( $\text{BC}_3$  and  $\text{B}_4\text{C}$ ) become stronger, which is agree with the literature.<sup>44</sup> With the increase of B doping amount, the content of B-C bonding increase firstly and then decrease. However, the reason is still unknown, which is needed further research.

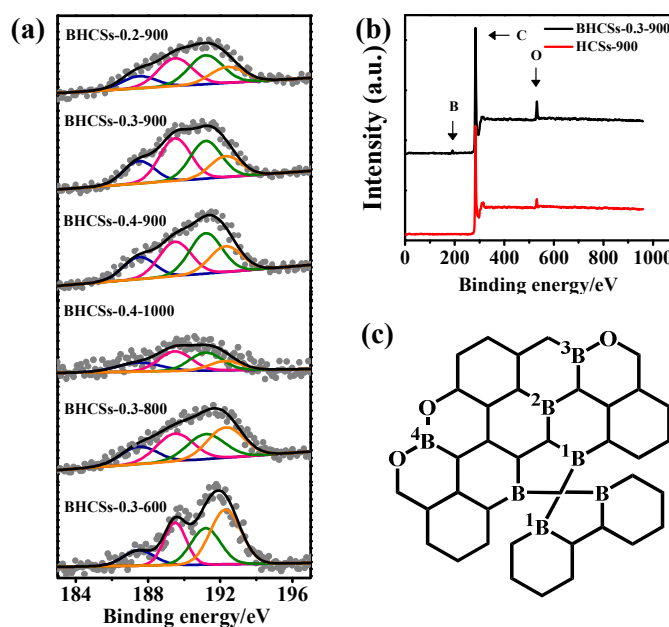


**Fig. 2** (a) XPS spectrum of HCSs-900 (black) and BHCSs-0.3-900 (red). (b) High resolution B1s XPS spectrum of BHCSs-0.3-700, BHCSs-0.3-800 and BHCSs-0.3-900. The B1s peak was accordingly deconvoluted into four peaks at 187.5 ( $\text{B}_4\text{C}$ , blue line), 189.5 ( $\text{BC}_3$ , pink line), 191.2 ( $\text{BC}_2\text{O}$ , green line), 192.3 ( $\text{BCO}_2$ , orange line). (c) Possible types of structure in the BHCSs derived from XPS measurements. <sup>1</sup>B ( $\text{B}_4\text{C}$ ); <sup>2</sup>B ( $\text{BC}_3$ ); <sup>3</sup>B ( $\text{BC}_2\text{O}$ ); <sup>4</sup>B ( $\text{BCO}_2$ ).

**Table 2.** B Species Content of BHCSs Samples by XPS

	B Species Content (at. %)			
	$\text{B}_4\text{C}$	$\text{BC}_3$	$\text{BC}_2\text{O}$	$\text{BCO}_2$
HCS-0.2-900	19.33	30.95	32.02	17.70
HCS-0.3-900	19.23	32.14	31.59	17.11
HCS-0.4-900	17.99	28.10	32.97	20.94
HCS-0.3-1000	20.29	33.50	30.58	15.63
HCS-0.3-800	17.23	27.57	25.55	29.65
HCS-0.3-600	11.46	22.49	25.51	40.54

### Electrochemical behavior of BHCSs

The catalytic activity of BHCSs to ORR was evaluated by CVs in oxygen-saturated 0.1 M KOH. Fig. 3a portrays the electrochemical reduction of oxygen at HCSs-900 (black line) and BHCSs-0.3-900 (red line) electrodes. For comparison, the same mass of each catalyst was loaded on the electrode as well as the geometrical area of the electrode was used to calculate the current density. For the  $\text{N}_2$ -saturated solution, reduction peaks are negligible both for HCSs-900 (black dash line) and BHCSs-0.3-900 (red dash line). In the presence of oxygen, a remarkable reduction peak at -0.174 V is observed on the obtained BHCSs-0.3-900 electrode, showing a substantial reduction process, which is 70 mV positive than that of HCSs-900.

To further research the ORR process and estimate the transferred electron number ( $n$ ) per oxygen molecule, the rotating disk electrode (RDE) measures was used to investigate

the electrocatalytic activity of BHCSs towards ORR by linear sweep voltammetry (LSV). Fig. 3b shows the corresponding LSVs for HCSs, BHCSs with different mass of B precursor and Pt/C disk electrode in oxygen-saturated 0.1 M KOH electrolyte. The HCSs-900, BHCSs-0.2-900, BHCSs-0.3-900, BHCSs-0.4-900 and Pt/C electrodes showed ORR onset potential at around -0.173 V, -0.144 V, -0.109 V, -0.101 V and -0.009 V. However, different mass loadings of BHCSs-0.3-900 could lead to different onset potential (Fig. S3, ESI†). As a non-metal catalyst, the BHCSs-0.3-900 showed ORR activity with an onset potential of -0.101 V in alkaline media, which is comparable to the other heteroatom doped carbon materials (Table S1, ESI†). As well as the obvious positive shift of the onset potential, the current density of BHCSs-0.3-900 was much stronger than that of HCSs-900. With the increase of B doping amount, the electrocatalytic activity of the BHCSs-900 meliorates initially and then deteriorates. Compared with BHCSs-0.2-900, the enhancement in the cathodic response of BHCSs-0.3-900 was ascribed to the increasing B content. However, it should be noted that the electrocatalytic activity of BHCSs-0.4-900 does not improve as expected. This may be caused by low surface area and low content of B-C bonding, especially BC<sub>3</sub> composition.

Tremendous reports showed that a high temperature around 600–1000 °C is vital for a successful graphitization and B implantation with optimal ORR catalytic activity.<sup>31,33,44</sup> Therefore, in this paper, four different calcination temperatures were investigated. Fig. 3b showed the onset potential and the current density enhanced obviously with the increase of temperature. The BHCSs-0.3-600, BHCSs-0.3-800, BHCSs-0.3-900 and BHCSs-0.3-1000 electrodes showed ORR onset potential at around -0.189 V, -0.133 V, -0.101 V and -0.137 V, respectively. Although with the increase of temperature, the surface area of the samples decreased, probably due to the collapse of pores and enhanced orientation during the carbonization process, the efficient active sites (B-C bonding) and the increase of graphitization armed the BHCSs-0.3-900 with higher catalytic activity. However, when the temperature is arrived at 1000 °C, due to the low B content and surface area, the electrocatalytic activity of the BHCSs deteriorates.

The detailed voltammograms at different rotation rates of BHCSs-0.3-900 were shown in Fig. 3c. The measured current density ( $J$ ) was improved with the increase of rotation rate ( $\omega$ ) for the shortened diffusion layer. Koutecky–Levich plots revealed good linearity between  $J^{-1}$  and  $\omega^{-1/2}$  and approximately constant slopes over the potentials from -0.3 to -0.8 V (Inset of Fig. 3c). The electron transfer number ( $n$ ) and kinetic current density ( $J_k$ ), two important parameters which reflect the kinetics of ORR process, are calculated from the slope and the reciprocal of the intercept of the K-L plots, respectively. According to the Koutecky–Levich equations (equation (1)–(3), ESI†), the calculated  $n$  value of BHCSs-0.3-900 is 3.7 at -0.6 V (Fig. 3d) and increased to 4 at more negative potentials (Fig. S4), indicating that oxygen reduction followed primarily the 4 electron pathway by reducing oxygen directly to OH<sup>-</sup>. By contrast, the value of  $n$  for HCSs at -0.6 V is 2.4, demonstrating

the oxygen reduction is a mainly 2 electron process with the formation of intermediate HO<sub>2</sub><sup>-</sup> ions. The calculated kinetic current density of BHCSs-0.3-900 is 6.91 mA cm<sup>-2</sup> while kinetic current density of HCSs-900 is 4.06 mA cm<sup>-2</sup> at -0.6 V. All these results indicate that doping B into the carbon framework endows the materials a better electrocatalytic activity to ORR than that of the pristine HCSs.

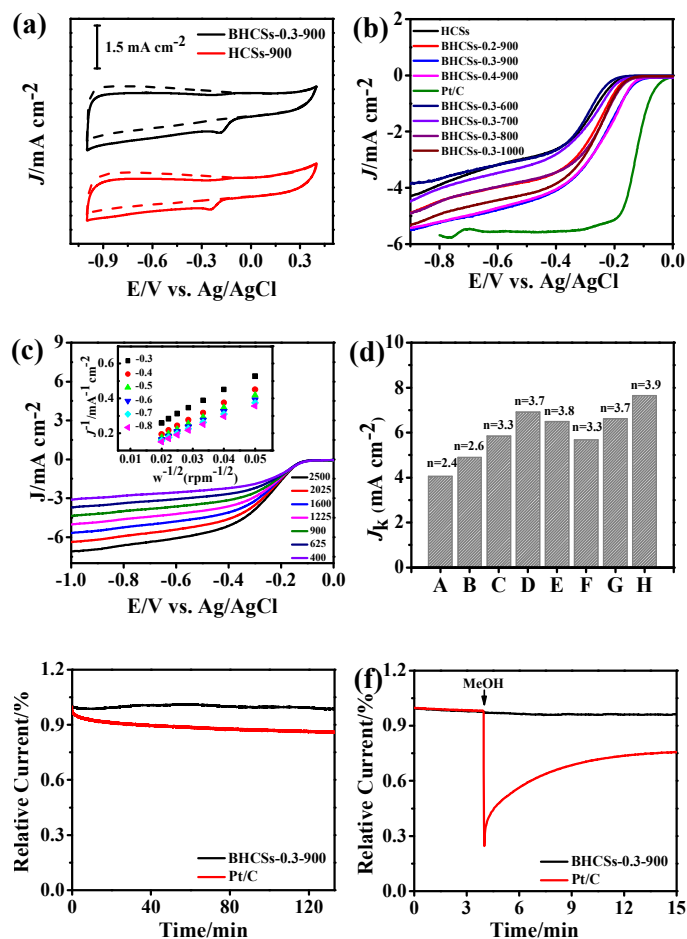


**Fig. 3** (a) CVs for BHCSs-0.3-900 and HCSs-900 on a glassy carbon rotating disk electrode in O<sub>2</sub>-saturated 0.1 M KOH solution with scan rate of 10 mV s<sup>-1</sup>. (b) Rotating-disk voltammograms of HCSs-900, various BHCSs samples, Pt/C in O<sub>2</sub>-saturated 0.1 M KOH with a scan rate of 10 mV s<sup>-1</sup> and rotation rate of 1600 rpm. (c) Rotating-disk voltammograms of BHCSs-0.3-900 in O<sub>2</sub>-saturated 0.1 M KOH with a sweep rate of 10 mV s<sup>-1</sup> at the different rotation rates. Inset: The corresponding Koutecky–Levich plot of  $J^{-1}$  versus  $\omega^{-1/2}$  from -0.3 to -0.8 V. (d) Summary of the kinetic limiting current density and the electron-transfer number on the basis of the RDE data on various catalysts. A (HCSs-900); B (BHCSs-0.3-600); C (BHCSs-0.3-800); D (BHCSs-0.3-900); E (BHCSs-0.3-1000); F (BHCSs-0.2-900); G (BHCSs-0.4-900); H (Pt/C). (e) Chronoamperometry of BHCSs-0.3-900 and Pt/C electrodes in O<sub>2</sub>-saturated 0.1 M KOH at -0.3 V for 130 min with the rotation rate of 1600 rpm. (f) Chronoamperometric responses of BHCSs-0.3-900 and Pt/C electrodes with 3 M methanol added at 4 min with the rotation rate of 1600 rpm.

The durability of the catalysts is also of major concern in fuel cells. Another attractive feature of the BHCSs catalysts is their highly steady amperometric response to ORR. The stability of BHCSs-0.3-900 and Pt/C catalysts in O<sub>2</sub>-saturated 0.1 M KOH was evaluated by chronoamperometry at -0.35 V with the electrode rotation rate at 1600 rpm. After 8000 seconds, the commercial Pt/C catalysts exhibited a loss of 15 % of the catalytic activity (Fig. 3e) while the BHCSs-0.3-900 remained stable throughout the experiment, with only 1.5% current diminution (Fig. 3e). Besides the excellent durability of the catalysts towards ORR, BHCSs-0.3-900 also shows good methanol tolerance. As shown in Fig. 3f, addition of 3 M methanol to the O<sub>2</sub> saturated electrolyte didn't apparently affect the catalytic activity of BHCSs-0.3-900 towards ORR (Fig. 3f). While the Pt/C catalyst displays a dramatic decay of relative current. This result clearly shows that BHCSs-0.3-900 selectively reduces O<sub>2</sub>, which is of benefit to avoid the occurrence of mixed potential in methanol fuel cells.

## Conclusions

In conclusion, BHCSs were synthesized from polymerized SiO<sub>2</sub> supported boric phenolic resin by carbonization of the latter, followed by etching away the SiO<sub>2</sub> template. BHCSs exhibited outstanding catalytic activity for ORR with better long-term stability and higher selectivity than commercial Pt/C catalysts in alkaline electrolytes. Furthermore, we discussed the role of B content, active sites, specific surface areas and calcination temperature in oxygen reduction process. The results demonstrate that BHCSs is a promising metal-free catalyst to ORR in fuel cells and other catalytic applications.

## Acknowledgements

This work was financially supported by the National Natural Science Foundation of China (Nos. 21035002, 21121091 and 21005016) and the Natural Science Foundation of Jiangsu Province (No. BK2011591).

## Notes and references

Jiangsu Province Hi-Tech Key Laboratory for Bio-medical Research, School of Chemistry and Chemical Engineering, Southeast University, Nanjing 210096, China. Fax: +86-25-52090618; Tel: +86-25-52090613; E-mail address: yingli@seu.edu.cn; liusq@seu.edu.cn.

† Electronic Supplementary Information (ESI) available. See DOI: 10.1039/b000000x/

- H. A. Gasteiger, N. M. Markovic. *Science*, 2009, **324**, 48-49.
- M. K. Debe. *Nature*, 2012, **486**, 43-51.
- N. Daems, X. Sheng, I. F. J. Vankelecom, P. P. Pescarmona. *J. Mater. Chem. A*, 2014, **2**, 4085-4110.
- R. G. Cao, J. S. Lee, M. L. Liu, J. Cho. *Adv. Energy Mater.*, 2012, **2**, 816-829.
- Y. Y. Liang, Y. G. Li, H. L. Wang, H. J. Dai. *J. Am. Chem. Soc.*, 2013, **135**, 2013-2036.
- Y. H. Bing, H. S. Liu, L. Zhang, D. Ghosh, J. J. Zhang. *Chem. Soc. Rev.*, 2010, **39**, 2184-2202.

- Y. J. Li, Y. J. Li, E. B. Zhu, T. McLouth, C. Y. Chiu, X. Q. Huang, Y. Huang. *J. Am. Chem. Soc.*, 2012, **134**, 12326-12329.
- Y. H. Bing, H. S. Liu, L. Zhang, D. Ghosh, J. J. Zhang. *Chem. Soc. Rev.*, 2010, **39**, 2184-2202.
- Z. L. Liu, X. H. Lin, J. Y. Lee, W. D. Zhang, M. Han, L. M. Gan. *Langmuir*, 2002, **18**, 4054-4060.
- A. Morozan, B. Josselme, S. Palacin. *Energy Environ. Sci.*, 2011, **4**, 1238-1254.
- H. X. Chang, H. K. Wu. *Energy Environ. Sci.*, 2013, **6**, 3483-3507.
- A. Ambrosi, C. K. Chua, A. Bonanni, M. Pumera. *Chem. Rev.*, 2014, **114**, 7150-7188.
- Y. Zhao, L. J. Yang, S. Chen, X. Z. Wang, Y. W. Ma, Q. Wu, Y. F. Jiang, W. J. Qian, Z. Hu. *J. Am. Chem. Soc.*, 2013, **135**, 1201-1204.
- E. J. Yoo, J. J. Nakamura, H. S. Zhou. *Energy Environ. Sci.*, 2012, **5**, 6928-6932.
- Y. M. Liu, S. Chen, X. Quan, H. M. Zhao, H. T. Yu, B. Y. Zhang. *J. Mater. Chem. A*, 2013, **1**, 14706-14712.
- D. W. Kim, O. L. Li, N. Saito. *Phys. Chem. Chem. Phys.*, 2015, **17**, 407-413.
- Y. M. Liu, S. Chen, X. Quan, H. T. Yu, H. M. Zhao, Y. B. Zhang, G. H. Chen. *J. Phys. Chem. C*, 2013, **117**, 14992-14998.
- L. Wang, P. Yu, L. Zhao, C. G. Tian, D. Y. Zhao, W. Zhou, J. Yin, R. H. Wang, H. G. Fu. *Sci. Rep.*, 2014, **4**, 5184-5192.
- Y. J. Zhang, K. Fugane, T. Mori, L. Niu, J. H. Ye. *J. Mater. Chem.*, 2012, **22**, 6575-6580.
- B. Zheng, J. Wang, F. B. Wang, X. H. Xia. *J. Mater. Chem. A*, 2014, **2**, 9079-9084.
- W. J. Jiang, J. S. Hu, X. Zhang, Y. Jiang, B. B. Yu, Z. D. Wei, L. J. Wan. *J. Mater. Chem. A*, 2014, **2**, 10154-10160.
- X. Xu, S. J. Jiang, Z. Hu, S. Q. Liu. *ACS Nano*, 2010, **4**, 4292-4298.
- J. Wu, Z. R. Yang, Q. J. Sun, X. W. Li, P. Strasser, R. Z. Yang. *Electrochim. Acta.*, 2014, **127**, 53-60.
- Y. Li, T. T. Li, M. Yao, S. Q. Liu. *J. Mater. Chem.*, 2012, **22**, 10911-10917.
- J. L. Shui, F. Du, C. M. Xue, Q. Li, L. M. Dai. *ACS Nano*, 2014, **8**, 3015-3022.
- D. S. Yang, D. Bhattacharjya, S. Inamdar, J. Park, J. S. Yu. *J. Am. Chem. Soc.*, 2012, **134**, 16127-16130.
- M. Seredych, T. J. Bandosz. *Carbon*, 2014, **66**, 227-233.
- Z. H. Sheng, H. L. Gao, W. J. Bao, F. B. Wang, X. H. Xia. *J. Mater. Chem.*, 2012, **22**, 390-395.
- H. Shi, Y. F. Shen, F. He, Y. Li, A. R. Liu, S. Q. Liu, Y. J. Zhang. *J. Mater. Chem. A*, 2014, **2**, 15704-15716.
- Y. Zheng, Y. Jiao, M. Jaroniec, Y. G. Jin, S. Z. Qiao. *Small*, 2012, **8**, 3550-3566.
- L. J. Yang, S. J. Jiang, Y. Zhao, L. Zhu, S. Chen, X. Z. Wang, Q. Wu, J. Ma, Y. W. Ma, Z. Hu. *Angew. Chem. Int. Ed.*, 2011, **50**, 7132-7135.
- X. J. Bo, L. P. Guo. *Phys. Chem. Chem. Phys.*, 2013, **15**, 2459-2465.
- G. Jo, S. Shanmugam. *Electrochem. Commun.*, 2012, **25**, 101-104.
- P. Rijiravanich, M. Somasundrum, W. Surareungchai. *Anal. Chem.*, 2008, **80**, 3904-3909.
- S. S. Feng, W. Li, Q. Shi, Y. H. Li, J. C. Chen, Y. Ling, A. M. Asiri, D. Y. Zhao. *Chem. Commun.*, 2014, **50**, 329-331.
- Y. Li, M. Yao, T. T. Li, Y. Y. Song, Y. J. Zhang, S. Q. Liu. *Anal. Methods*, 2013, **5**, 3635-3638.

- 37 T. Y. Yang, J. Liu, R. F. Zhou, Z. G. Chen, H. Y. Xu, S. Z. Qiao, M. J. Monteiro. *J. Mater. Chem. A*, 2014, **2**, 18139-18146.
- 38 G. P. Yin, Y. Z. Gao, P. F Shi, X. Q. Cheng, A. Aramata. *Mater. Chem. Phys.*, 2003, **80**, 94-101.
- 39 N. Li, Q. Zhang, J. Liu, J. Joo, A. Lee, Y. Gan, Y. D. Yin. *Chem. Commun.*, 2013, **49**, 5135-5137.
- 40 W. Stober, A. Fink, E. Bohn. *J. Colloid Inter. Sci.*, 1968, **26**, 62-69.
- 41 J. Liu, S. Z. Qiao, H. Liu, J. Chen, A. Orpe, D. Y. Zhao, G. Q. Lu. *Angew. Chem. Int. Ed.*, 2011, **50**, 5947-5951.
- 42 J. T. Jin, X. G. Fu, Q. Liu, Y. R. Liu, Z. Y. Wei, K. X. Niu, J. Y. Zhang. *ACS Nano*, 2013, **7**, 4764-4773.
- 43 R. Balgis, S. Sago, G. M. Anilkumar, T. Ogi, K. Okuyama. *Appl. Mater. Interfaces*, 2013, **5**, 11944-11950.
- 44 J. T. Jin, F. P. Pan, L. H. Jiang, X. G. Fu, A. M. Liang, Z. Y. Wei, J. Y. Zhang, G. Q. Sun. *ACS Nano*, 2014, **8**, 3313-3321.
- 45 C. Wang, Z. Y. Guo, W. Shen, Q. J. Xu, H. M. Liu, Y. G. Wang. *Adv. Funct. Mater.*, 2014, **24**, 5511-5521.